CORE
Metadata, citation and similar papers at core.ac.uk
Provided by UNT Digital Library

LBNL-61665

Invited Review

To be submitted to the

SPECIAL ISSUE OF

JOURNAL OF PHYSICS D: APPLIED PHYSICS

"PLASMA-AIDED NANOFABRICATION"

Nanostructures by Energetic Condensation of Metal Plasmas

André Anders

Lawrence Berkeley National Laboratory, University of California,

1 Cyclotron Road, Berkeley, California 94720

September 21, 2006

This work was supported by the Assistant Secretary for Energy Efficiency and Renewable Energy, Office of Building Technology, of the U.S. Department of Energy under Contract No. DE-AC02-05CH11231.

Metal plasmas for the fabrication of nanostructures

André Anders

Lawrence Berkeley National Laboratory, University of California,

1 Cyclotron Road, Berkeley, California 94720

Abstract

A review is provided covering metal plasma production, the energetic condensation of metal plasmas, and the formation of nanostructures using such plasmas. Plasma production techniques include pulsed laser ablation, filtered cathodic arcs, and various forms of ionized physical vapor deposition, namely magnetron sputtering with ionization of sputtered atoms in radio frequency discharges, self-sputtering, and high power impulse magnetron sputtering. The discussion of energetic condensation focuses on the control of kinetic energy by biasing and also includes considerations of the potential energy and the processes occurring at subplantation and implantation. In the final section on nanostructures, two different approaches are discussed. In the top-down approach, the primary nanostructures are lithographically produced and metal plasma is used to coat or fill trenches and vias. Additionally, multilayers with nanosize periods (nanolaminates) can be produced. In the bottom-up approach, thermodynamic forces are used to fabricate nanocomposites and nanoporous materials by decomposition and dealloying.

Keywords: metal plasma, energetic condensation, subplantation, metallization, multilayers, nanolaminates, nanocomposites, nanoporous metal, decomposition

1. Introduction

Metal plasmas and nanostructures have been around for a long time but only in recent years one has been able to recognize the greater potential of their applications, enabled by progress in fabrication, metrology, high resolution microscopy, and synergy with the developments of neighboring disciplines. The term “nanostructure” is understood here in a rather broad sense, namely, wherever nanometer-size features play a role for the properties and applications. Both the top-down (involving lithography) and the bottom-up approach (involving self-organization) will be considered.

This review will start with generation methods for metal plasmas, with emphasis on various forms of ionized physical vapor deposition (i-PVD), including high power impulse magnetron sputtering (HIPIMS) and filtered cathodic vacuum arc (FCVA) deposition. Although *metal* plasmas are the focus of this review, semimetals like carbon (graphite) and semiconductors are considered, too, as long as these materials have enough conductivity to be utilized in an arc or sputter process. After the plasma formation has been considered, review deals with the processes of energetic condensation involving metal ions, the formation of intermixed layers, self-ion-assisted deposition of ultrathin films, multilayers of ultrathin films, also known as nanolaminates, the formation of nanoparticles in films (nanocomposites) and on surfaces (islands, nanoparticles), and the metallization and filling of lithographically produced trenches and vias.

2. Generation of metal plasmas suitable for the fabrication of precise coatings and nanostructures

2.1 Pulsed Laser Deposition

The ablation and ionization of solid target material has been used for many years and in facts was (and still is) the main fabrication technique for high temperature superconducting films (like $YBa_2Cu_3O_{3-x}$ or "YBCO") and devices such as SQIDs (superconducting quantum interference devices).

High laser power density on the target surface is required to accomplish the phase transition from solid to plasma. The degree of ionization mainly depends mainly on the power density and also on the laser pulse length. The solid target material can be conducting or insulating (in contrast to the later-discussed arc and sputter methods), and the process can be done in vacuum or in a background gas, giving it great flexibility. The plasma plume from the target expands and the ablated particles can condense on a substrate placed nearby, a process generally called pulsed laser deposition (PLD). High quality films can be obtained, for example crystalline ZnO [1] or doped ZnO and GaN films [2]. There are many similarities (and some differences) to pulsed cathodic arcs. Like cathodic arcs, the origin of the plasma source is point-like (the focal point of the laser beam), and the threshold power density is comparable to the power density of cathode spots [3]. The point-like emission of the plasma plume leads to non-uniform coatings unless controlled motion of the substrate and/or the source point is implemented. PLD has the advantages of good control and reproducibility. It is an excellent tool for high-value-added structures and R&D purposes [4, 5] but it is not widely used for industrial coatings due to high cost and low average deposition rates. For further information, the reader is referred to the reviews [6, 7].

2.2 Filtered cathodic arcs

Cathodic arcs are characterized by plasma formation at non-stationary cathode spots [8-10]. Detailed investigations point to fractal properties in time and space down to the nanosecond and micrometer range, implying extremely high momentary power densities (~ 10^{13} W/m^2 or even greater) [11]. As a consequence, the plasma is fully ionized with multiply charged ions [12], although neutrals exist, too, originating from sources other than the cathode spot, such as evaporating macroparticles and non-sticking, neutralized ions.

A well-known drawback of cathodic arcs is the presence of the so-called macroparticles, which are a by-product of the microexplosions at cathode spots. Fig. 1 shows the size distribution of macroparticles, which is very broad compared to nanoparticles intentionally produced by other methods such as clusters nucleated and grown in relatively dense gas atmosphere. Therefore, cathodic arc macroparticles have not (yet?) been considered for practical use.

For precision coating and nanostructure formation, macroparticles need to be removed from the streaming metal plasma, and this has been accomplished by a variety of filtering techniques. The most prevalent is the use of a curved solenoid: the magnetic field is sufficient to magnetize electrons, setting up a transverse electric field which in turn confines and guides the ions. The combined action of magnetic and electric field can guide the streaming plasma from the source to a substrate. The macroparticles are removed because they are too massive to be noticeably affected by the fields. The technique was introduced in the late 1970s in the former Soviet Union [13], and is now widely used with a great variety of geometries – for reviews on filters see [14-16].

The separation of macroparticles from the metal plasma can be clearly observed in open solenoid filters (Fig. 2). For high-tech applications, where macroparticle removal must be as perfect as possible, double bend or curvatures greater than 90° are utilized, for example in the S-filter [17], the off-plane double bend (OPDB) filter duct [18], the open Twist Filter [19] , the 120° filter [20], and the elongated S-filter for rectangular cathodes [21].

2.3 Ionized physical vapor deposition (i-PVD) based on post-sputter ionization

The shrinking dimensions of computer chips lead to increasingly demanding metallization techniques. Conventional magnetron sputtering could not satisfy the needs of the mid 1990s, when the feature size shrunk to 500 nm, and certainly it is completely unsuitable for today's 90-65 nm, or the near future 45 nm feature sizes. It was quickly recognized that the wide range of incident angles of condensing atoms lead to closure (plug-up) of the trench or via before they were filled. In a next improvement, only those sputtered atoms were utilized that move almost perpendicular to the surface; this was realized by using condensing plates or tubes placed parallel to the axis between target and substrate. However, besides being not very economical, this "long throw sputtering" could not satisfy demands. The need for providing a highly directed beam of condensing particles with well controlled energy was recognized. Acceleration of sputtered particles in one direction was needed, which could be accomplished if the sputtered atoms become ionized. That was the driving force for the development of ionized physical vapor deposition (i-PVD) [22].

Sputtered atoms have a few eV of kinetic energy and therefore travel very quickly from the target; the likelihood of ionization is low unless they are slowed down. Therefore, i-PVD processes operate at relatively high gas pressure to ensure slowing of the sputtered atoms by elastic collisions with gas atoms, and subsequent ionization of sputtered material via inelastic collisions with energetic particles (mainly electrons). Additional power for the ionization is supplied by RF (radio frequency) heating of electrons, preferably by an ICP (inductively coupled plasma) produced between target and substrate. The original "throwing power" of sputtering is sacrificed but directed flux is not obtained by acceleration in the electric field of the sheath. The ionization processes and the metallization of nanostructures were modeled and are now well understood [23], see also section 4.1.

2.4 Ionized PVD based on self-sputtering

For a few materials, like copper and silver, the exceptional combination of high self-sputter yield and high rate of ionization enables the sputtering in the self-sputter mode. The process can be started as usual with argon gas. Once sputtering has started, and sufficient power is supplied, a good fraction of the sputtered atoms is ionized and contributes to sputtering if returned to the target. At high powers, the sputtering by returning metal ions can be so significant that the gas contribution is no longer needed, and in fact, the gas supply can be shut off [24]. Although limited to some metals only, the process is relevant because it works for copper, which is a preferred material for metallization due to its high electrical conductivity.

2.5 Ionized PVD based on high power impulse magnetron sputtering (HIPIMS)

Self-sputtering is also a critical and enabling process in the emerging technology of high power impulse magnetron sputtering. Before going into the technical details, some clarification is needed for the terminology used. Mid-frequency "pulsed-DC magnetron sputtering" or short "pulse sputtering" is used when peak power densities on the target surface are moderate (~ 10 W/cm^2) and repetition frequencies are relatively high (typically up to 300 kHz). In the recent literature, the term "high power pulsed magnetron sputtering" (HPPMS) is used with two different meanings, namely, (i), for mid-frequency, pulsed-DC magnetron sputtering applied to large areas, leading to many 10 kW of total (average) power [25] yet moderate peak power densities of several 10 W/cm^2, and (ii), to pulsed sputtering with relatively low pulse repetition rates (1 kHz or less) with extremely high peak power, typically hundreds of kW or even MW, corresponding to peak power densities of typically 1 kW/cm^2, or even greater. To distinguish between these forms of pulsed sputtering, the term "high power impulse magnetron sputtering" (HIPIMS) was introduced, referring to a process using very high peak power at relatively low repetition rates [26].

For HIPIMS, the limitation in the repetition rate is dictated by the average power handling (cooling) of the magnetron. During each pulse, the flux of sputtered atoms grows to large values, and the high power invested leads to high ionization; up to 70% is claimed in extreme cases [27]. One should recall that for many applications, one does not need full ionization. An ionization level of some 10% is already significant, leading to qualitatively different films and structures, especially if the energy of ions is increased by biasing.

In contrast to self-sputtering in continuous mode, HIPIMS is a highly dynamic process that requires a certain level of gas, usually argon (for metal deposition), or argon mixed with a desirable reactive gas (for compound formation). The noble gas argon can be replaced by others, like the heavier krypton, but this is usually not done for economical reasons. During each pulse, a relatively high voltage (~ 1 kV) is applied that drives the discharge current to high levels (~ 1 kA), much exceeding the continuously sustainable levels known from DC or medium-frequency pulsed-DC sputtering.

The discharge is not an arc as evidenced by the discharge voltage which remains typically in the 500 V range. It is measured between anode and cathode, and should not to be confused with the open-circuit voltage. If arcing occurs, the voltage sharply drops, while the current may slightly or greatly increase, depending on the impedance of the circuit. This is a clear difference to magnetron discharges at lower power levels, where a sudden, significant increase in discharge current can always serve as a discriminator for the onset of arcing. Once arcing has started, highly ionized metal plasma is produced including undesirable macroparticles: after all, the process is now a cathodic arc, as discussed before. Conditions for arcing and arc suppression have been described in the literature [25, 28, 29]. Modern power supplies are equipped with sophisticated and fast (~ 1 μs) arc detection and termination circuits that enable application of HIPIMS even to the very important and challenging reactive systems like aluminum oxide [30] and zirconium oxide and tantalum oxide [31]. However, one should recall that arc spots can ignite and operate down to the nanosecond range [32-34], thus very small arc damage and small amounts of macroparticles should be expected. The level of damage can be low and is acceptable to many applications like hard, wear resistant coatings [35].

The degree of ionization of the sputtered atoms is a function of time, as all of the parameters are. Approximate determination using optical emission spectroscopy and plasma particle monitoring reveal high peak values, often approaching or even exceeding 50% [27].

3. Energetic condensation

3.1 Definition

After having described the most important approaches to form metal plasmas, or mixed metal-gas plasmas, we can now move on to look at the substrate side of the process, where energetic condensation processes in combination with thermodynamic driving forces lead to a wealth of thin films, nanolayers, and nanostructures materials.

Energetic condensation can be defined as a condensation process where hyperthermal particles play a critical role. "Hyperthermal" refers to particles whose kinetic energy is much greater than the average thermal energy, and in particular energies greater than the bulk displacement energy of the substrate material. The latter is defined as the energy needed to move a substrate atom from its bulk lattice site to a stable interstitial site. The bulk displacement energy is not well defined because it depends on the direction of the energetic particle causing the displacement relative to the crystalline texture, if the material is crystalline, and for amorphous materials, the terms "interstitial" and "vacancy" can only be understood in the sense of local density. Therefore, a range of energies exists for the creation of a Frenkel pair (interstitial and vacancy). Displacement energies are typically in the range from about 10 eV (e.g. for magnesium) to about 40 eV (e.g. for rhenium) [36]. The uncertainty in the definition of the displacement energy

should not be of great concern because the arriving particles have broad energy distribution functions, and much higher energies can be involved. The point is that processes occur not just on the surface but involve the immediate subsurface region, with great consequences on the condensing films in terms of density, stress, textures, hardness, etc. Additionally, considering lithographically produced 3-D nanostructures, impact angles other than normal are present. Ions impacting under oblique angles and at high energies may cause enhanced self-sputtering and exhibit a low sticking coefficient. These effects enabled filling of high aspect ratio trenches and vias, see section 4.1.

3.2 Biasing: Control of the kinetic energy by acceleration in sheaths

The most important motivation of using *plasma*, as opposed to a flux of sputtered atoms, neutral vapor or gas, is the ability to influence the kinetic energy of ions via an electric field, thereby enabling the effects of energetic condensation. Let us consider the simplest case, namely a conducting substrate facing a plasma without an external magnetic field. Biasing the substrate negatively relative to the plasma potential causes the formation of a sheath adjacent to the substrate (a low voltage sheath with $V_s \sim kT_e/e$ exists in the absence of bias but here we focus on bias effects). If the curvature of the substrate is negligible, the sheath thickness is given by Child's law

$$d = \frac{2}{3}\left(\frac{2\,\varepsilon_0^2\,V_s^3}{\overline{Q}e\,kT_e\,n_{i0}^2}\right)^{1/4}, \qquad (1)$$

where V_s is the sheath voltage, $\overline{Q}$ is the average ion charge state number (for cathodic arcs, see tables in [37]), T_e and n_{i0} are the electron temperature and the ion density at the sheath edge, respectively, e is the elementary charge, and ε_0 is the permittivity of free

space. A positive ion arriving at the sheath edge with kinetic energy $E_{kin,0}$ will be accelerated and arrives at the surface with the kinetic energy

$$E_{kin}(Q,t) = E_{kin,0} + Q\,V_{bias}(t) \tag{2}$$

provided there are no collisions in the sheath (refinements to this expression will be discussed later). From this equation one can see that the charge state Q plays an important role: whereas neutral atoms will not "feel" the sheath, the energy gain for ions is directly proportional to their charge state. All of the previously mentioned metal plasmas may contain multiply charge states. In particular, almost all cathodic arc plasmas contain multiply charged ions, and especially the charge state distribution of refractory metals have fractions of 4+ and even 5+. Therefore, even with a modest bias voltage of say 100 V, the kinetic energy can exceed 400 or even 500 eV, causing significant sputtering and emission of secondary electrons, and a low sticking probability if the impact occurs at large angles to the surface normal.

3.3 Additional heating by potential energy

The ions arriving at the surface do not only carry kinetic energy but also potential energy, which can be significant to local, atomic-scale heating, thereby affecting the properties of the growing structure [38].

The potential energy of ions includes the excitation energy of bound electrons, E_{exc}, the cohesive energy, E_c, and the (cumulative) ionization energy. Let's look at each of these contributions.

The excited states may be Boltzmann distributed (equilibrium assumption, dense plasmas) or underpopulated (excitational non-equilibrium of low density plasmas). In

any case, the contribution of excitation energy to heating is small and therefore it can be neglected.

In contrast, the ionization energies can be significant, especially for multiply charged ions. The ionization energy, E_Q, is defined as the energy needed to remove a bound electron from an ion of charge state Q, forming an ion of charge state to Q+1 (Ref. [39]). When calculating the heating effect, the cumulative ionization energy needs to be considered,

$$E_{Q+}^{cum} = \sum_{Q'=0}^{Q-1} E_{Q'} \quad . \tag{3}$$

When the arriving ion becomes incorporated in a growing film, the cohesive energy becomes available. The cohesive energy, E_c, is defined as the energy needed to remove an atom from its bulk position in the solid to an infinitely distant position. The cohesive energy ranges from 1.5 to 8.9 eV.

The cumulative ionization energies are the most relevant of all potential energies, and can reach large values for multiply charged ions, e.g. 151 eV for W^{5+}. Data for the cumulative ionization energies and cohesive energies of all relevant metal ions are tabulated in Ref [38].

3.4. Refinements: Image charge, and stepwise neutralization

An ion approaching a surface goes through several stages before becoming inserted into the sub-surface zone (near normal incidence) or being reflected (large off-normal angle impact). For a metal surface, the approaching ion generates an image charge of opposite polarity, exerting the force

$$F = (eQ)^2 \Big/ \left(4\pi\varepsilon_0 (2d)^2\right) \quad (4)$$

where d is the distance between the ion and the surface, leading to acceleration towards the surface. With decreasing distance, the electric field of the ion reduces the potential barrier that normally keeps conduction band electrons from escaping into the vacuum. In the classical "over-the-barrier" (COB) model [40], electrons near the Fermi edge of the metal can transfer resonantly into an excited level of the incident ion when the potential barrier between metal and the ion reaches the Fermi level, i.e., when the transfer becomes classically allowed. The transfer occurs at a critical distance

$$d_c(Q) \approx a_B E_H \Big/ \phi\sqrt{8Q+2} \quad (5)$$

where a_B is the Bohr radius, E_H is the ionization energy of hydrogen and ϕ is the work function. After the transfer, the ion charge and the image charge are reduced and the barrier height increased. If the ion had only one charge, it is now an energetic atom. In the case of a multiply charged ion, a second, smaller critical distance exists where a second electron transition is classically allowed; i.e., multiply charged ions reduce their charge stepwise in a staircase fashion. In the staircase approximation, the kinetic energy gain by image charge is [40]

$$E_{ic} = \frac{\phi}{2} \sum_{i=0}^{Q-1} \frac{2(Q-i)-1}{\sqrt{8(Q-i)+2}} \,. \quad (6)$$

For example, a gold ion of charge state Q=3 approaching a gold surface ($\phi \approx 5.4$ eV) will gain kinetic energy by image charge acceleration of $E_{ic} \approx 10.8$ eV. One can see that this energy is large compared to the threshold energies for atom diffusion on the surface but small compared to the energy gained by acceleration in the sheath's electric field. The energy gain by image charge acceleration is even smaller when the ion

approaches an insulating surface [41], and therefore does not need to be further considered here.

3.5 Subplantation and plasma immersion ion implantation

When the ion (or energetic atom, or "hollow atom" originated from multiply charged ions) arrives at the surface, the projected range of penetration is determined by its kinetic energy. The so-called stopping power of the material is of order 100 eV/nm, determined by (i) nuclear elastic collisions, involving large, discrete energy losses with significant angular deflection of the ion trajectory in the solid, and (ii) electronic inelastic collisions where the moving ion excites or ejects electrons of the substrate, involving small energy losses per collision and negligible deflections of the ion trajectory [42]. At the relatively low energies considered in energetic condensation, nuclear stopping is dominant [43].

If the atoms are inserted just below the surface, the process is often called subplantation [44]. Subplantation is widely investigated for the growth of tetrahedral amorphous carbon (ta-C, e.g. [45, 46]). At higher ion energies and thus greater depth, the process may be described as (shallow) ion implantation. Because ions are directly extracted from the plasma, and if high sheath voltages (typically kV in a pulsed mode) are involved, the process is commonly labeled as plasma immersion ion implantation (PIII) (handbook [47] and references therein). The effects of ion implantation such as concentration depth profile can readily be calculated by Monte Carlo codes, such as the well-known TRIM code [48]. For high fluence situations, subplantation, and film growth one need to use one of the dynamic versions like TRIDYN [49] or T-DYN [50].

“Dynamic” means the code accounts for changes in the substrate caused by the ions: ions arriving later in the process see a solid that is already modified by the ions that have arrived so far. While Monte Carlo is computationally very fast, one needs to employ much more elaborate Molecular Dynamics simulations to study the atomic collision cascades and displacements in great detail [51-53].

4. Metal plasmas for top-down nanostructures

4.1. Metallization

In the top-down approach to nanostructures, a lithographic technique is used to create an initial structure. For example, integrated circuits are fabricated using sub-100 nm structures to obtain very high density of processing elements. Several plasma techniques have been developed to “wire” these elements after magnetron sputtering and long throw sputtering has been shown to be inadequate (Fig. 3). Ionized magnetron sputtering (section 2.3) was the first of the successful techniques for sub-micrometer features (see section 2.3 above) [22, 23, 54]. The processes of conformal coating or filling of trenches and vias rely on the energy and angle-depend sputter yields and sticking coefficients. Ion impact at higher energies and off-normal angles lead to enhanced sputtering (Fig. 4), while the sticking probability becomes very small when the angle exceeds about 60° (Fig.5) [55].

Since the requirements specified a highly directional metal flux relative to the structure, it is quite natural to consider filtered cathodic arc plasma. The first report on filling of trenches having a width down to 400 nm and a depth-to-width aspect ratio of 2 came from Siemroth and coworkers [56] in Dresden, Germany. They used their filtered

high current pulsed arc (φ-HCA) with copper, and they also demonstrated conformal coating of 1 μm wide low aspect ratio structures. Although important, these results could not yet represent a viable alternative to the then-used tungsten chemical vapor deposition (CVD) for feature sizes of 350 nm. Later improvements were demonstrated by the Dresden group (Fig. 6) but were not widely publicized. Monteiro [57] in Berkeley, California, reported on improved results using a plasma technique involving a miniature filtered pulsed arc source and the application of high-duty-cycle pulsed bias on the substrate. He demonstrated conformal coating of Ta and TaN diffusion barrier and Cu seeding layers in 120 nm wide trenches and vias with aspect ratios of up to 8:1 (Fig. 7), and the complete filling of trenches with copper (Fig. 8). Similar results have been obtained more recently by Chen and Shih [58] in Taiwan. These results suggest that even smaller, sub-100 nm features might be possible.

4.2. Graded layers, ultrathin films, multilayers, nanolaminates

The energetics of the ion condensation process can be utilized to form interlayers and graded layers of desirable thickness and composition. Brown and coworkers [59, 60] phased metal plasma production and bias pulses, giving periods of lower energy (no or low bias voltage) and high energy (subplantation or implantation, depending on the level of bias voltage), which resulted in very adherent films with a broadened substrate-film interlayer. This approach developed into Metal Plasma Immersion Ion Implantation and Deposition (MePIIID) [61], characterized by the use of metal plasmas in conjunction with pulsed and variable substrate bias.

The high bias, and related high ion energy, lead to substrate-film mixing at the interface, which was originally attributed to be the main reason for superior adhesion [62], especially for materials that can form strong chemical bonds. For example, energetic condensation of carbon on silicon leads to a thin silicon carbide ("glue") interlayer. More recent research identified stress relaxation as a main contributor to improved adhesion because the forces on the interface are greatly reduced. Bilek and McKenzie [63] developed a comprehensive model for the observation that stress, hardness and other properties of many materials show a maximum in the energetic condensation when the energy is in the range of about 100 eV, whereas the properties are reduced when a (even small) percentage of arriving ions has high energy (e.g. keV). This is due to a relaxation process that involves many substrate atoms per incident ions.

Of special interest is carbon because it has the ability to form materials of vastly different properties depending on the bonding (large sp^2 versus sp^3), on the structure (amorphous versus crystalline), and the presence of other elements (hydrogen, carbide-forming or non-carbide-forming elements). This field is huge, and the reader is referred to the many reviews and research papers, e.g. [4, 64, 65]. Here, only the example of carbon-carbon nanolayered structures should be mentioned. Such material can be obtained using the MePIIID approach by periodically varying the bias on the substrate, hence periodically varying the energy of arriving carbon ions [66]. High bias in the kV range leads to films of lower density and lower sp^3 content (Fig. 9). Other fabrication options include the periodic relaxation of the growing film [67]. In any case, the mechanical properties of the complete structure, such as elastic modulus, hardness, stress, and fracture toughness, depend on both the properties of the individual layers as well as

on the period of the structure; e.g., periods of thinner films lead to an increase in hardness [68]. Studies at elevated temperature (600°C) showed that the high density layers were not greatly affected by annealing, whereas low density layers develop strong preferred orientation either as a result of elevated deposition temperatures or post deposition annealing [69].

Intermixing of film and substrate on the one hand and the synthesis of ultrathin (few nm thick) films on the other represents conflicting requirements when the desired film thickness approaches the thickness of intermixed layer. This question is especially important for the deposition of ultrathin ta-C films as wanted for protective coatings in the data storage industry [70-74]. Lower energy will reduce the thickness of the intermixed layer but the energetic conditions for sp^3-rich material would be violated. Simulations indicate that it is impossible to obtain ta-C films thinner than 2 nm [75]; thinner films will be either intermixed or do not show a high sp^3 content.

The avoidance of intermixing between layers is also of critical importance to X-ray optics multilayers. While energetic condensation of carbon is desirable to make a dense low-Z material, the high-Z material must not be deposited in an energetic way [76, 77].

Plasma-deposited nitride-based nanolaminates and superlattices play an important role for many tribological applications such as cutting tools and engines.

For example, Hultman and coworkers [78] surveyed TiN/NbN superlattices research and concluded that plastic deformation and dislocation glide is limited to within individual layers in scratching experiments. Superlattice hardening is attributed to dislocation confinement with barriers to dislocation glide across the layer interfaces.

Quaternary nitride (Ti,Cr,Al)N/WN nano-multilayered coatings were shown to result in a significant increase of tool life as well as wear behavior improvement under conditions of dry high-speed machining (end milling) of hardened H13 steel (HRC 50) [79]. The nano-multilayered coatings showed enhanced tribological adaptability because W-O tribo-films form in synergy to alumina and other phases. Hardening is often associated with the formation of nanocrystallites, which leads to the topic of the next section.

5. Metal plasmas for bottom-up nanostructures: decomposition and self-organization

5.1. Nanocomposites

Metal plasmas play also an important role in the formation of certain kinds of nanostructures. Low temperature (incl. room temperature) condensation of plasma of metal and metal alloys is a process far from thermodynamic equilibrium. Therefore one can produce thin films, or multilayer coatings, that are metastable material systems. Under specific conditions, such as high temperature developing under load when used, the material can decompose and form self-organized nanostructured materials. This is now widely used to produce superhard ($H > 40$ GPa) and tough surfaces [80, 81]. The superior mechanical properties are associated with the formation of nanocrystallites that are usually embedded in an amorphous matrix of the other material, so-called nanocomposites.

PLD, arc plasma deposition and magnetron sputtering are used to fabricate these advanced materials. Using titanium-aluminum and titanium-zirconium cathodes,

multilayer composite films have been deposited since the 1990s using cathodic arc plasma deposition [82]. XPS (x-ray photoemission spectroscopy) of the material strongly suggested that the (TiAlN) films contained TiN and AlN phases, and correspondingly (TiZr)N contained TiN and ZrN phases. Today it is established that the popular hard coating material TiAlN exhibits spinodal decomposition resulting in distinct TiN and AlN phases . Mayrhofer and coworkers [83] showed that metastable $Ti_{1-x}Al_xN$ coatings initially undergo spinodal decomposition into coherent cubic-phase nanometer-size domains, causing an increase in hardness at elevated temperatures. These intermediate metastable domains transform into their stable phases TiN and AlN during further thermal treatment. This mechanism of age hardening at high temperature is agreement with very recent *ab initio* calculations [84]. Annealing studies (700-900°C) of nano-crystalline $Al_{0.67}Ti_{0.33}N$ coatings deposited by cathodic arcs showed nanossize domains of c-AlN in a c-(Ti, Al)N matrix which helped to maintain the high hardness of the material upon annealing while the reduced defect density resulted in lower surface damage during wear and an improvement in tool life [85].

Another example of advanced, adaptive nanoscale multilayer structures is a superlattice of the type TiAlCrN/TiAlYN with typical period of 1.7 nm [86]. The incorporation of yttrium not only improved the oxidation resistance but also effectively reduced the coefficient of friction of the coating from 0.9 to 0.65 at temperatures in the range of 850–950°C. It was found that the adaptation of the tribological properties occurs as a result of the preferential migration of yttrium to the column boundaries. Similarly, incorporation of vanadium leads to a self-adaptation process in the TiAlN/VN nanosize superlattice. During friction, the coatings adapt themselves to the combined

thermal and mechanical wear by the formation of highly lubricious vanadium-oxides due to high flash temperatures at the asperity contacts on the surface. The integrity of the bulk of the coating is retained, leading to exceptionally low, for superhard coatings, friction coefficient of 0.5 and a wear coefficient of 2×10^{-17} $m^3 \cdot N^{-1} \cdot m^{-1}$ [86].

5.2 Nanoporous materials

A very different example of nanostructure formation by decomposition is when one of the decomposed materials is volatile. The result is generally a highly porous material. For example, nanostructures porous platinum, a “platinum sponge” can be synthesized by plasma deposition of metastable platinum oxide (Fig. 10). Both magnetron sputtering [87] and filtered arc (unpublished) have been demonstrated to be suitable for the deposition of the to-be-decomposed material, and perhaps other processes far from thermodynamic equilibrium may work as well. Metastable platinum oxide can be decomposed by providing the activation energy in form of elevated temperature, or by exposing the oxide to hydrogen, which reduces the compound [88]. The resulting structure with pore sizes in the 10s to 100s of nm is very similar to nanoporous gold obtained by electrochemical dealloying of AgAu alloy [89]. Decomposition and dealloying appear to be rather general approaches for the fabrication of nanoporous materials, and plasma deposition is a suitable (but not the only possible) route to making the starting material.

5.3 Dewetting and nanoscale islands

Another example of self-organization can occur directly on the surface, namely the formation of islands for non-wetting conditions. This phenomenon is not limited to the condensation of metal plasmas but can also occur by condensation from the vapor phases. Though, the presence of plasma and the arrival of energetic particles modifies the structures because the motion of particles on the surface is promoted, thereby reaching a state closer to thermodynamic equilibrium. In any case, if the condensing material does not wet the surface of the substrate, it tends to form islands as shown in Fig.   (fig of silver), with significant consequences for the electrical, optical and mechanical properties. Nanosized islands can also be obtained when a non-wetting film was deposited at low temperature and the system is annealed at elevated temperature or by exposure to plasma: the film will break up and form islands by dewetting [90]. Nanosized islands, or nanoparticles, on surfaces can be used to achieve desirable catalytic effects and spectrally selective absorption of light.

6. Summary and Outlook

Metal plasmas can be produced by a number of techniques; most of them involve an electrical discharge. The feedstock material is usually one the electrodes, and in many cases the cathode (magnetron sputtering, cathodic arcs). Self-sputtering is among the critical processes that need to be considered in both the formation of metal ions and their interaction with the substrate/film surface. Often, the power density is high and multiply charged metal ions are present, which is important considering the energetics of the condensation process. Substrate bias is a common route to increase the energy of

condensing ions, leading to subplantation or even implantation, depending on the voltage level of the bias.

Metal plasmas and vapors have been used in both the top-down and bottom-up approach to nanostructures. In the former, lithography is used to provide the primary structure that is further modified, and here we discuss in particular metallization of the pattered semiconductors for integrated circuit fabrication. Both trench filling and conformal coating down to the 100 nm feature size has been demonstrated. The mechanisms are on the energy and angle depended self-sputtering features of metal.

Nanosize interlayers and graded structures can be produced by intermixing of condensing ions and substrate. Highly adherent coatings have been obtained, and recent research indicated the critical role of stress relaxation by energetic ion impact.

In the bottom-up approach, metal plasmas are often used in nanosized compound multilayers that can undergo phase changes at elevated temperature. Dislocation glide is limited to within individual layers, and spinodal decomposition lead to nanocomposites that have exceptionally high hardness, especially when used at high temperatures. Decomposition and dealloying leads to nanoporous materials if one or more of the decomposed materials are volatile. In this way, nanosponge films of noble metals have been fabricated. Finally, nanostructures can also be obtained on the surface utilizing the effects of nonwetting and dewetting.

The plasma properties such as flux density of ions to a substrate, ion energy, combination of various species, etc. represent important "knobs" for tuning the properties of materials, interfaces, films, and structures. Using advanced diagnostics and characterization techniques, as well as computational models, the field is poised to be

used in a wider range of applications, for example in the fabrication of photonic and biomedical devices.

Acknowledgements

The author would like to thank Peter Siemroth for providing the data for figures 1, 3, and 6; Othon Monteiro kindly provided figures 7 and 8. Sunnie Lim is gratefully acknowledged for his SEM work (Fig. 10). This work was supported by the Assistant Secretary for Energy Efficiency and Renewable Energy, Office of Building Technology, of the U.S. Department of Energy under Contract No. DE-AC02-05CH11231.

References

[1] Misra P and Kukreja L M *Thin Solid Films* 2005 **485** 42-46.

[2] Dorneles L S, O'Mahony D, Fitzgerald C B, McGee F, Venkatesan M, Stanca I, Lunney J G, and Coey J M D *Appl. Surf. Sci.* 2005 **248** 406-410.

[3] Vogel N and Höft H *IEEE Trans. Plasma Sci.* 1989 **17** 638-640.

[4] Voevodin A A and Donley M S *Surf. Coat. Technol.* 1996 **82** 199-213.

[5] Voevodin A A, Jones J G, and Zabinski J S *J. Appl. Phys.* 2000 **88** 1088-1096.

[6] Miller J C (Ed.) *Laser Ablation: Principles and Applications*. Berlin and New York: Springer, 1994.

[7] Chrisey D B and Hubler G K (Ed.) *Pulsed Laser Deposition of Thin Films*. New York: Wiley, 1994.

[8] Boxman R L, Sanders D M, and Martin P J, *Handbook of Vacuum Arc Science and Technology*. Park Ridge, N.J.: Noyes Publications, 1995.

[9] Mesyats G A, *Cathode Phenomena in a Vacuum Discharge: The Breakdown, the Spark, and the Arc*. Moscow, Russia: Nauka, 2000.

[10] Anders A, *Cathodic Arc Plasma Deposition: From Fractal Spots to Energetic Condensation (in preparation)*. New York: Springer Inc., 2007.

[11] Anders A *IEEE Trans. Plasma Sci.* 2005 **33** 1456-1464.

[12] Anders A and Yushkov G Y *J. Appl. Phys.* 2002 **91** 4824-4832.

[13] Aksenov I I, Belous V A, Padalka V G, and Khoroshikh V M *Sov. J. Plasma Phys.* 1978 **4** 425-428.

[14] Anders A *Surf. Coat. Technol.* 1999 **120-121** 319-330.

[15] Martin P J and Bendavid A *Thin Solid Films* 2001 **394** 1-15.

[16] Boxman R L and Zhitomirsky V N *Rev. Sci. Instrum.* 2006 **77** 021101-15.

[17] Anders S, Anders A, Dickinson M R, MacGill R A, and Brown I G *IEEE Trans. Plasma Sci.* 1997 **25** 670-674.

[18] Shi X, Tay B G, and Lau S P *Int. J. Mod. Phys. B* 2000 **14** 136-153.

[19] Anders A and MacGill R A *Surf. Coat. Technol.* 2000 **133-134** 96-100.

[20] Siemroth P, Personal Communication, 2003.

[21] Zhitomirsky V N, Boxman R L, and Goldsmith S *Surf. Coat. Technol.* 2004 **185** 1-11.

[22] Rossnagel S R and Hopwood J *J. Vac. Sci. Technol. B* 1994 **12** 449-453.

[23] Hopwood J A (Ed.) *Ionized Physical Vapor Deposition*. San Diego, CA: Academic Press, 2000.

[24] Posadowski W M and Radzimski Z *J. Vac. Sci. Technol. A* 1993 **11** 2980-2984.

[25] Krause U, List M, and Fuchs H *Thin Solid Films* 2001 **392** 196-200.

[26] Ehiasarian A P, Hovsepian P E, Hultman L, and Helmersson U *Thin Solid Films* 2004 **457** 270-277.

[27] Bohlmark J, Alami J, Christou C, Ehiasarian A, and Helmersson U *J. Vac. Sci. Technol. A* 2005 **23** 18-22.

[28] Sproul W D, Christie D J, and Carter D C *Thin Solid Films* 2005 **491** 1-17.

[29] Anders A *Thin Solid Films* 2006 **502** 22-28.

[30] Sproul W D, Christie D J, and Carter D C, “The reactive sputter deposition of aluminum oxide coatings using high power pulsed magnetron sputtering (HPPMS),” 47th Annual Technical Conference, Society of Vacuum Coaters, Dallas, TX, 2004, 96-100.

[31] Glocker D A, Romach M M, Christie D J, and Sproul W D, "High power pulsed reactive sputtering of zirconium oxide and tantalum oxide," 47th Annual Technical Conference, Society of Vacuum Coaters, Dallas, TX, 2004, 183-186.

[32] Jüttner B *J. Phys. D: Appl. Phys.* 2001 **34** R103-R123.

[33] Barengolts S A, Mesyats G A, and Shmelev D L *IEEE Trans. Plasma Sci.* 2003 **31** 809-816.

[34] Jüttner B *IEEE Trans. Plasma Sci.* 1999 **27** 836-844.

[35] Ehiasarian A P, Munz W D, Hultman L, Helmersson U, and Petrov I *Surf. Coat. Technol.* 2003 **163-164** 267-272.

[36] Eckstein W, *Computer Simulation of Ion-Solid Interactions*. Berlin: Springer-Verlag, 1991.

[37] Anders A *Phys. Rev. E* 1997 **55** 969-981.

[38] Anders A *Appl. Phys. Lett.* 2002 **80** 1100-1102.

[39] Carlson T A, Nestor C W, Wasserman N, and McDowell J D *Atomic Data* 1970 **2** 63-99.

[40] Burgdörfer J and Meyer F *Phys. Rev. A* 1993 **47** R20-R22.

[41] Hägg L, Reinhold C O, and Burgdörfer J *Nucl. Instrum. Meth. Phys. Res. B* 1997 **125** 133-137.

[42] Nastasi M, Mayer J W, and Hirvonen J K, *Ion-Solid Interactions*. Cambridge, UK: Cambridge University Press, 1996.

[43] Ziegler J F, Biersack J P, and Littmark U, *The Stopping and Range of Ions in Solids*. New York: Pergamon Press, 1985.

[44] Lifshitz Y, Kasai S R, Rabalais J W, and Eckstein W *Phys. Rev. B* 1990 **41** 10468-10480.

[45] Jäger H U and Belov A Y *Phys. Rev. B* 2003 **68** 024201-13.

[46] Gago R, Jimenez I, Albella J M, Climent-Font A, Caceres D, Vergara I, Banks J C, Doyle B L, and Terminello L J *J. Appl. Phys.* 2000 **87** 8174-8180.

[47] Anders A (Ed.) *Handbook of Plasma Immersion Ion Implantation and Deposition*. New York: John Wiley & Sons, 2000.

[48] Ziegler J F and Biersack J P, "Computer code TRIM: *Transport of Ions in Matter , version 92.24*," 1992.

[49] Möller W, Eckstein W, and Biersack J P *Comp. Phys. Comm.* 1988 **51** 355-368.

[50] Biersack J P *Nucl. Instrum. Meth. Phys. Res. B* 1991 **59/60** 21-27.

[51] Diaz de la Rubia T, Averback R S, Hsieh H, and Benedek R *J. Mater. Res.* 1989 **4** 579-586.

[52] Hubler G K and Sprague J A *Surf. Coat. Technol.* 1996 **81** 29-35.

[53] Uhlmann S, Fraunheim T, and Lifshitz Y *Phys. Rev. Lett.* 1998 **81** 641-644.

[54] Nichols C A, Rossnagel S M, and Hamaguchi S *J. Vacuum Sci. Technol. B* 1996 **14** 3270-3275.

[55] Hanson D E, Stephens B C, Saravanan C, and Kress J D *J. Vac. Sci. Technol. A* 2001 **19** 820-825.

[56] Siemroth P, Wenzel C, Kliomes W, Schultrich B, and Schülke T *Thin Solid Films* 1997 **308** 455-459.

[57] Monteiro O R *J. Vac. Sci. Technol. B* 1999 **17** 1094-1097.

[58] Chen U-S and Shih H C *Nucl. Instrum. Meth. Phys. Res. B* 2005 **237** 477-483.

[59] Brown I G, Godechot X, and Yu K M *Appl. Phys. Lett.* 1991 **58** 1392-1394.

[60] Brown I G, Anders A, Anders S, Dickinson M R, Ivanov I C, MacGill R A, Yao X Y, and Yu K-M *Nucl. Instrum. Meth. Phys. Res. B* 1993 **80/81** 1281-1287.

[61] Anders A *Surf. Coat. Technol.* 1997 **93** 157-167.

[62] Anders A, Anders S, Brown I G, Dickinson M R, and MacGill R A *J. Vac. Sci. Technol. B* 1994 **12** 815-820.

[63] Bilek M M M and McKenzie D R *Surf. Coat. Technol.* 2006 **200** 4345-4354.

[64] Robertson J *Prog. Solid State Chem.* 1991 **21** 199-334.

[65] Chhowalla M, Robertson J, Chen C W, Silva S R P, Davis C A, Amaratunga G A J, and Milne W I *J. Appl. Phys.* 1997 **81** 139-145.

[66] Anders S, Callahan D L, Pharr G M, Tsui T Y, and Bhatia C S *Surf. Coat. Technol.* 1997 **94/95** 189-194.

[67] Friedmann T A, Sullivan J P, Knapp J A, Tallant D R, Follstaedt D M, Medlin D L, and Mirkarimi P B *Appl. Phys. Lett.* 1997 **71** 3820-3822.

[68] McKenzie D R, Tarrant R N, Bilek M M M, Ha T, Zou J, McBride W E, Cockayne D J H, Fujisawa N, Swain M V, James N L, Woodard J C, and McCulloch D G *Diamond Rel. Mat.* 2003 **12** 178-184.

[69] McCulloch D G, Xiao X L, Peng J L, Ha P C T, McKenzie D R, Bilek M M M, Lau S P, Sheeja D, and Tay B K *Surf. Coat. Technol.* 2005 **198** 217-222.

[70] Anders S, Brown I G, Bhatia C S, and Bogy D B *Data Storage* 1997 **4** 31-38.

[71] Robertson J *Tribology International* 2003 **36** 405-415.

[72] Jacoby B, Wienss A, Ohr R, von Gradowski M, and Hilgers H *Surf. Coat. Technol.* 2003 **174-175** 1126-1130.

[73] Casiraghi C, Ferrari A C, Ohr R, Chu D, and Robertson J *Diamond Rel. Mat.* 2004 **13** 1416-1421.

[74] Piazza F, Grambole D, Schneider D, Casiraghi C, Ferrari A C, and Robertson J *Diamond Rel. Mat.* 2005 **14** 994-999.

[75] Anders A and Kulkarni A V *Proc. Mat. Res. Soc.* 2001 **675** paper W11.1-12.

[76] Anders S, Anders A, Kortright J B, M. Y K, Brown I G, and Ivanov I C *Surf. Coat. Technol.* 1993 **61** 257-261.

[77] Baranov A M *Optics Communications* 1999 **167** 23-26.

[78] Hultman L, Engstrom C, Birch J, Johansson M P, Oden M, Karlsson L, and Ljungcrantz H *Zeitschrift fur Metallkunde* 1999 **90** 803-813.

[79] Fox-Rabinovich G S, Yamamoto K, Veldhuis S C, Kovalev A I, Shuster L S, and Ning L *Surf. Coat. Technol.* 2006 **201** 1852-1860.

[80] Veprek S *J. Vac. Sci. Technol. A* 1999 **17** 2401-2420.

[81] Musil J *Surf. Coat. Technol.* 2000 **125** 322-330.

[82] Sant S B and Gill K S *Surf. Coat. Technol.* 1994 **68-69** 152-156.

[83] Mayrhofer P H, Hörling A, Karlsson L, Sjolen J, Larsson T, Mitterer C, and Hultman L *Appl. Phys. Lett.* 2003 **83** 2049-2051.

[84] Mayrhofer P H, Music D, and Schneider J M *Appl. Phys. Lett.* 2006 **88** 071922-3.

[85] Fox-Rabinovich G S, Endrino J L, Beake B D, Kovalev A I, Veldhuis S C, Ning L, Foitane F, and Gray A *Surf. Coat. Technol.* 2006 **In Press, Corrected Proof**.

[86] Hovsepian P E, Lewis D B, Luo Q, Munz W-D, Mayrhofer P H, Mitterer C, Zhou Z, and Rainforth W M *Thin Solid Films* 2005 **485** 160-168.

[87] Maya L, Riester L, Thundat T, and Yust C S *J. Appl. Phys.* 1998 **84** 6382-6386.

[88] Maya L, Brown G M, and Thundat T *J. Appl. Electrochem.* 1999 **29** 883-888.

[89] Erlebacher J, Aziz M J, Karma A, Dimitrov N, and Sieradzki K *Nature* 2001 **410** 450-453.

[90] Dannenberg R, Stach E, Groza J R, and Dresser B J *Thin Solid Films* 2000 **359** 1-9.

Figure captions

Fig. 1 Size distributions of copper macroparticles as determined by microscopy with different magnification. The power law supports a fractal interpretation of spot processes. The leveling-off at small size was determined to be an artifact of the measuring technique (data provided by Peter Siemroth).

Fig. 2 Open-shutter photograph of an open solenoid filter illustrating the separation of macroparticles from the metal (actually, here carbon) plasma; the pulsed plasma source is on the right hand side; the straight line is the path of an exceptionally large, glowing-hot macroparticle coming from the graphite cathode and bouncing off from one of the turns of the filter.

Fig. 3 Incomplete filling of trenches by long-throw sputtering (figure courtesy of P. Siemroth).

Fig. 4 Self-sputter yield as a function of impact angle and ion energy; the data shown refer to simulation for nickel but they are representative for other materials, too (adapted from [55]).

Fig. 5 Sticking probability of ions as a function of impact angle and ion energy; the data shown refer to simulation for nickel but they are representative for other materials, too (adapted from [55]).

Fig. 6 Deposition of a Cu layer on a submicrometer semiconductor (figure courtesy of P. Siemroth).

Fig. 7 Conformal coating of a 120 nm trench with Ta using the MePIIID technique with optimized pulsed bias (figure courtesy of O. Monteiro).

Fig. 8 Filling of a trench with copper using the MePIIID technique with optimized pulsed bias (figure courtesy of O. Monteiro).

Fig. 9 Cross section TEM of a carbon-carbon multilayer produced by MePIIID: the dark (denser layer was deposited with a pulsed bias of -100 V while the lighter (less dense) layer was made with -2000 V pulsed bias. (Adapted from [66])

Fig. 10 Nanoporous platinum "sponge" film, about 2 μm thick, produced by decomposition of plasma-deposited platinum oxide.

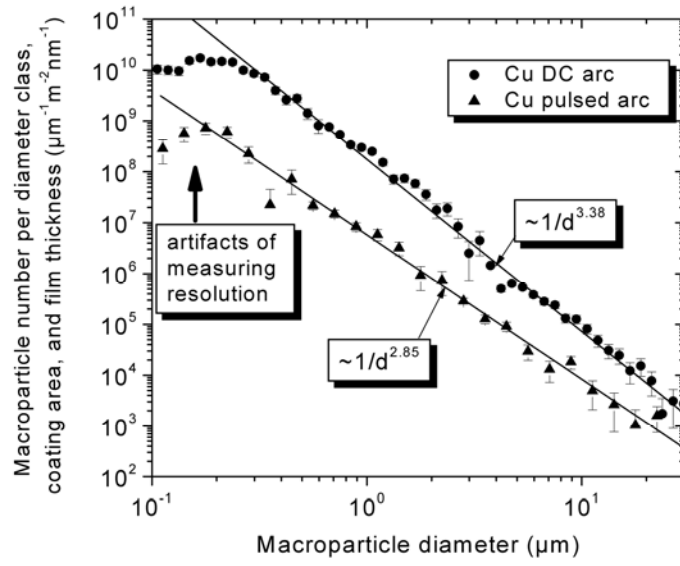

Fig. 1

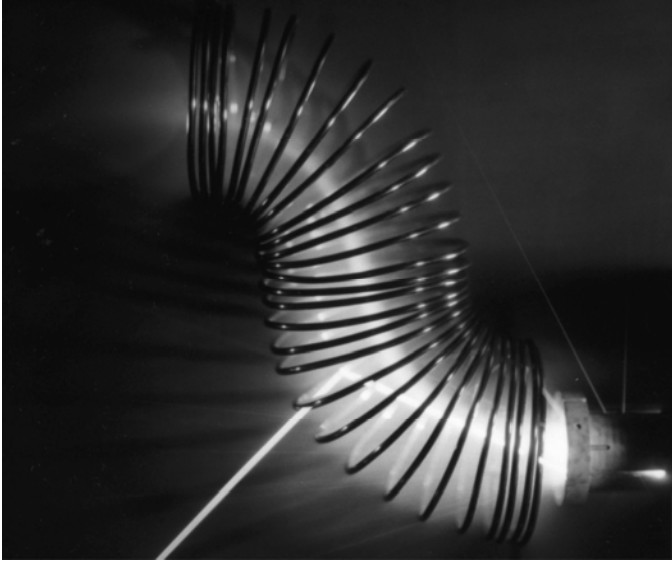

Fig. 2

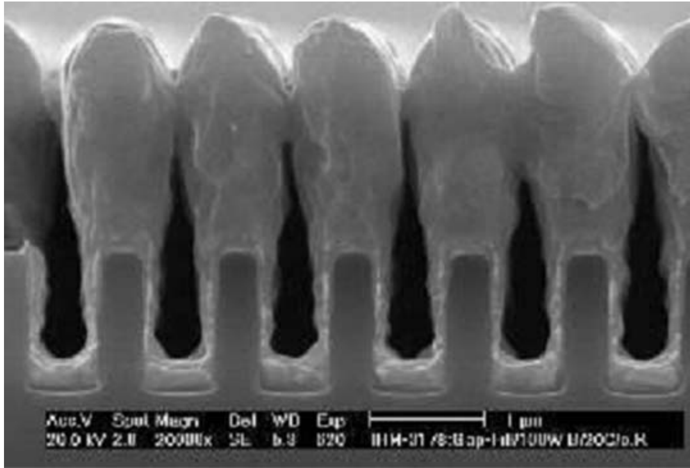

Fig. 3

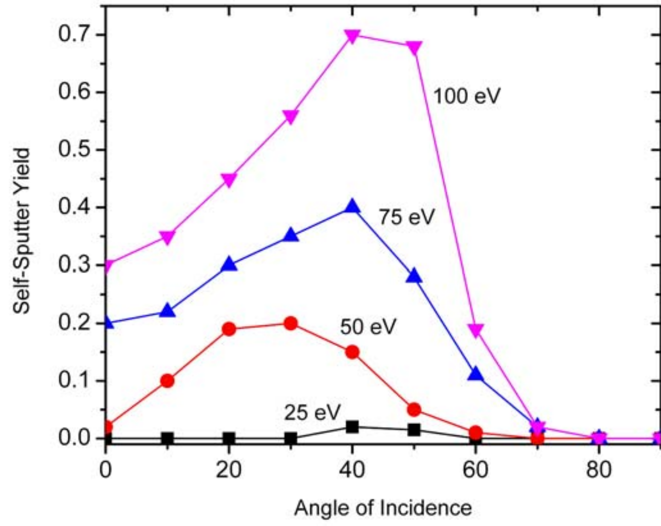

Fig. 4

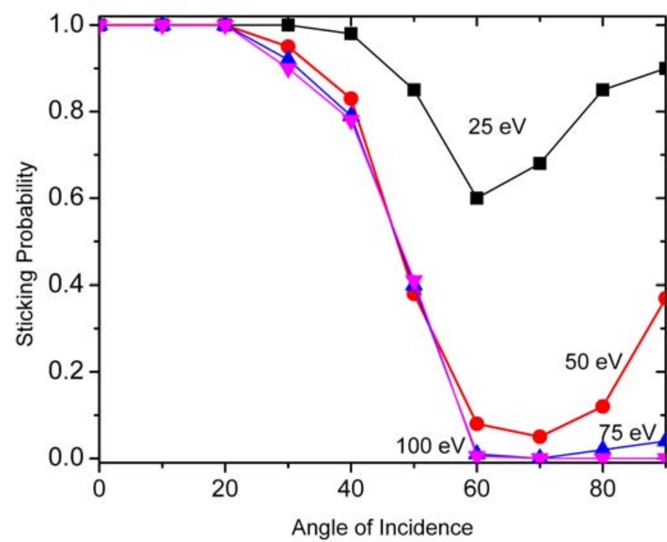

Fig. 5

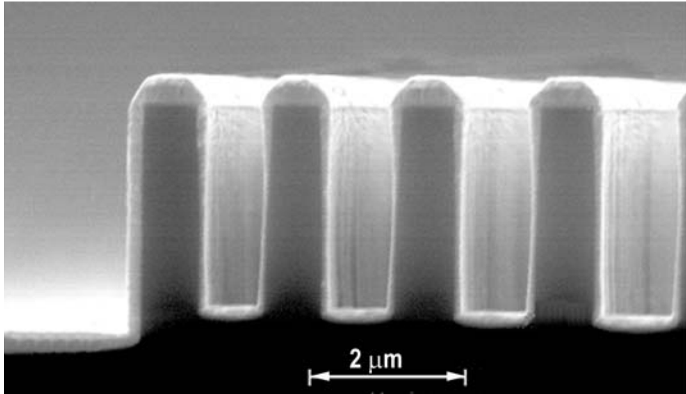

Fig. 6

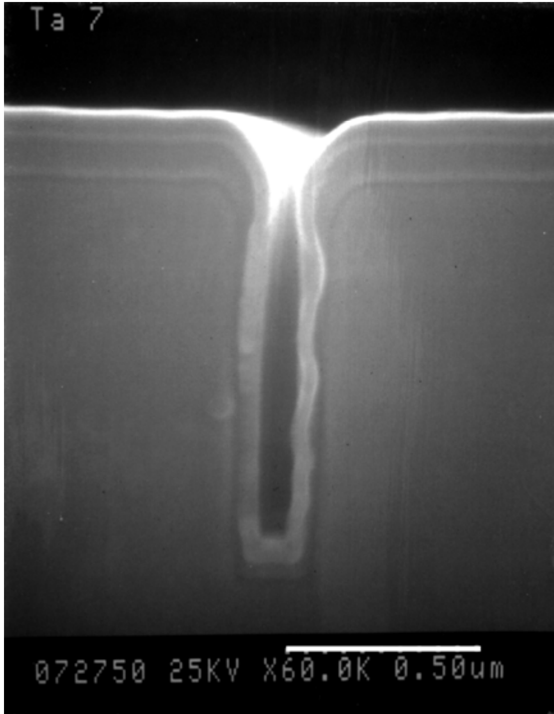

Fig. 7

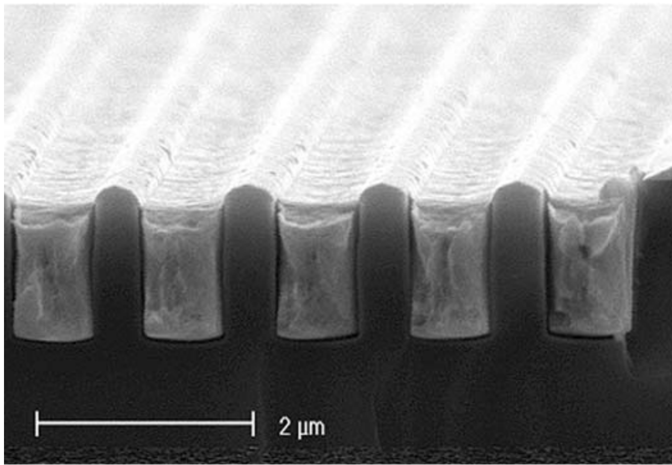

Fig. 8

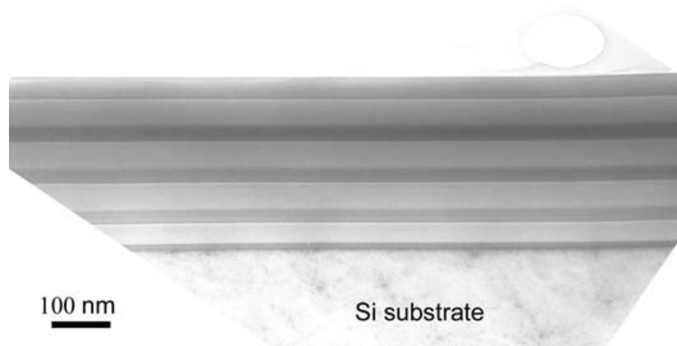

Fig. 9

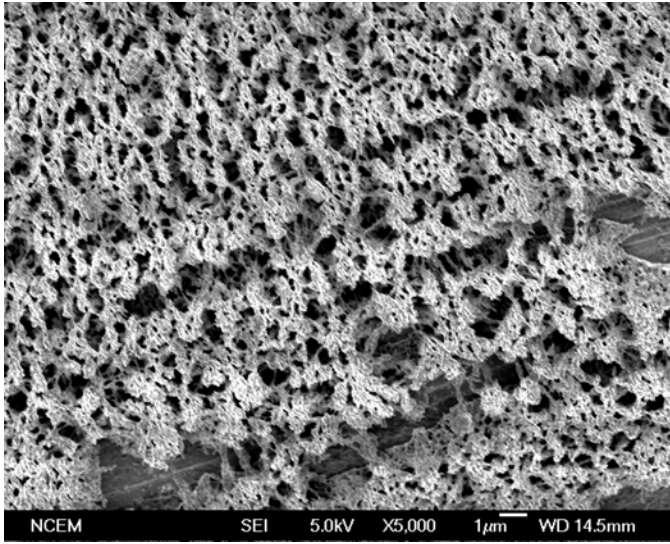

Fig. 10